On the local energy conservation of a system of three unidirectionally coupled undamped forced Duffing oscillators and their dynamics

I. A. Alvarado-López and F. J. Carmona-Moreno

Departamento de Ciencias Exactas y Tecnología, Centro Universitario de los Lagos, Universidad de Guadalajara, Enrique Díaz de León 1144, Colonia Paseos de la Montaña, Lagos de Moreno, Jalisco, México.
e-mail: israel.alvarado3960@alumnos.udg.mx; felipe.carmona5766@alumnos.udg.mx

E. Urenda-Cázares

Departamento de Matemáticas, Centro Universitario de Ciencias Exactas e Ingenierías, Universidad de Guadalajara, Blvd. Gral. Marcelino García Barragán 1421, Colonia Olímpica, 44430 Guadalajara, Jalisco, México,
e-mail: ernesto.urenda@academicos.udg.mx

J. J. Barba-Franco

Departamento de Ciencias Básicas, Tecnológico Nacional de México,
Instituto Tecnológico José Mario Molina Pasquel y Henríquez
Calle José Guadalupe Tejeda Vázquez, Arandas, 47180 Jalisco, Mexico.
e-mails: jose.barba@arandas.tecmm.edu.mx; josedejesusbarbafranco@gmail.com

Received 13 May 2025; accepted 11 June 2025

The Duffing oscillator is a well-established model with broad applications in physics, engineering, and biological systems. This study examines a system of three undamped, non-autonomous Duffing oscillators arranged in a unidirectionally coupled ring configuration. The model enables the exploration of intricate dynamical behaviors, including multistability, synchronization, and the onset of chaos. Local energy conservation is analyzed through integrals of motion and phase-space examination, considering various coupling strengths and natural frequency parameters. By applying the Milne-Pinney equations, the study identifies three conserved quantities-each associated with an oscillator-whose interdependence reflects the structural influence of the ring. The findings demonstrate how unidirectional coupling and non-autonomous forcing facilitate energy exchanges within the system, revealing that local energy conservation is not merely a consequence of global symmetries but rather emerges from the complex interplay of nonlinear interactions. This deeper perspective enhances the understanding of energy dynamics in coupled oscillatory systems.

Keywords: Lagrangian; conserved quantities; coupled oscillators; undamped systems; phase space analysis.

DOI: https://doi.org/10.31349/RevMexFis.71.060702

1. Introduction

The Duffing oscillator is a nonlinear dynamic system that has been extensively studied since its introduction in 1918 by Georg Duffing [1]. Over the years, it has found applications across various fields, including physical systems [2-5], engineering [6-10], and biological systems [11,12], among others (see [13] and references therein).

Recently, its applications in coupled systems have gained relevance due to the rich dynamics that have allowed deepening in the multi-stability analysis, synchronization, and emergent chaotic behavior. In 2020, Barba-Franco *et al*. [14] studied the behavior of two unidirectionally and bidirectionally coupled Duffing oscillators, observing a synchronization dependent on the coupling strength. Subsequently, these results were used to analyze a unidirectionally tricoupled ring, incorporating different forms of time-dependent damping. This allowed the study of the multistability of the system, obtaining fixed-point stability and hyperchaos depending on the type of damping used [15]. Furthermore, in 2022, Uriostegui-Legorreta *et al*. [16] proposed a master-slave system in which they couple a Duffing oscillator and a Van der Pol oscillator under different coupling schemes, successfully achieving the synchronization of both oscillators. Finally, in 2023, Balaraman *et al*. [17] studied a tricoupled ring of Duffing oscillators, identifying 27 equilibrium points, from these diverse dynamics, leading to different behaviors such as limit cycles and chaotic spirals.

According to Noether's theorem, published in 1918 by Emmy Noether [18], every symmetry of a physical system corresponds to a conserved quantity. In other words, using the integral of motion, it is possible to obtain information about the system's symmetries and even the solution's stability properties without calculating them explicitly [19-22]. Integrals of motion have potential applications in nonlinear systems (see [23,24] and references therein). Techniques for finding integrals of motion are essentially based on algebraic arguments, Noether's theorem, or methods based on transformation groups [25,26].

The present work aims to analyze the behavior of a unidirectional tricoupled ring using undamped Duffing oscillators by varying the coupling strengths and natural oscillation parameters. The system dynamics are studied using space-time surfaces, time series, and phase portraits, following a similar approach to other investigations [27,28], where the Lagrangian of the system, together with Noether's theorem, are used to analyze symmetry transformations, as well as energy conservation through the integral of motion. In Urenda-Cázares *et al*. [27], a bidirectional tricoupled ring of Duffing oscillators is studied, where the Lagrangian and the integral of motion are employed to examine the behavior of the system. Chaotic or multistable dynamics are observed depending on the variation of the coupling parameters. For their part, Barba-Franco *et al*. [28] use the integral of motion to analyze a master-slave system of Duffing oscillators with nonlinear coupling, identifying the presence of chaos and synchronization as a function of the oscillation strength. This kind of coupled configuration may have future applications in the design and analysis of nonlinear signal transmission systems and energy transport in networked mechanical structures [29,30].

The paper is organized as follows: In Sec. 2 we explore the existence of conserved quantities for the unidirectionally coupled Duffing system. In Sec. 3 we present the numerical results obtained from integrating the system under different configurations of the natural frequency parameter. Three distinct cases were considered: constant frequency, sinusoidal variation, and quadratic variation. The time evolution of the solutions and local energy conservation are analyzed. Finally, these results illustrate how the dynamics of the system changes under various conditions of the frequency parameter. It has been observed that the unidirectional coupling introduces changes in the local energies of each node that depend on the diffusive coupling.

2. Model

In order to demonstrate the existence of conserved quantities for the model of an unidirectionally coupled Duffing system, specifically considering the undamped Duffing oscillator with an external force of modulation, first we use a single Duffing oscillator:

$$\ddot{x} + \Omega(t)x + \delta(t)x^3 = \Gamma(t), \tag{1}$$

where $\delta(t)$, $\Omega(t)$ and $\Gamma(t)$ are parameters of the system.

Figure 1 shows a three unidirectionally coupled Duffing oscillator system using a directed graph, where the vertices represent each oscillator and the edges represent their coupling ξ.

Taking Fig. 1 and using Eq. (1) in each node, the full second-order system result as follows

$$\begin{aligned}
&\ddot{x}_1 + \Omega(t)x_1 + \delta(t)x_1^3 + \xi\,(x_1 - x_3) = \Gamma_1(t),\\
&\ddot{x}_2 + \Omega(t)x_2 + \delta(t)x_2^3 + \xi\,(x_2 - x_1) = \Gamma_2(t),\\
&\ddot{x}_3 + \Omega(t)x_3 + \delta(t)x_3^3 + \xi\,(x_3 - x_2) = \Gamma_3(t),
\end{aligned} \tag{2}$$

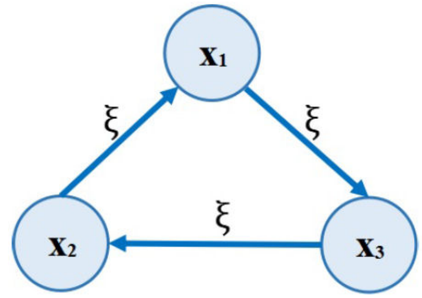

FIGURE 1. A ring of three Duffing oscillators unidirectionally coupled.

where ξ is the coupling strength coefficient. Note that diffusive coupling is included.

Now, to solve the equation system (2) is implemented an order reduction of $\dot{x}_j = y_j$ for $j = 1, 2, 3$. As a result, the system is transformed into a first-order equation system:

$$\begin{aligned}
&\dot{x}_1 = y_1,\\
&\dot{y}_1 = -\Omega(t)x_1 - \delta(t)x_1^3 - \xi\,(x_1 - x_3) + \Gamma_1(t),\\
&\dot{x}_2 = y_2,\\
&\dot{y}_2 = -\Omega(t)x_2 - \delta(t)x_2^3 - \xi\,(x_2 - x_1) + \Gamma_2(t),\\
&\dot{x}_3 = y_3,\\
&\dot{y}_3 = -\Omega(t)x_3 - \delta(t)x_3^3 - \xi\,(x_3 - x_2) + \Gamma_3(t).
\end{aligned} \tag{3}$$

Similarly to other work available in the literature [28], it is possible to propose a proper Lagrangian associated with (2). This Lagrangian is defined by

$$\begin{aligned}
L(x_1, \dot{x}_1, x_3,\ t) &= \frac{1}{2}m(t)\dot{x}_1^2 - V\,(x_1, x_3, t),\\
L(x_2, \dot{x}_2, x_1,\ t) &= \frac{1}{2}m(t)\dot{x}_2^2 - V\,(x_2, x_1, t),\\
L(x_3, \dot{x}_3, x_2,\ t) &= \frac{1}{2}m(t)\dot{x}_3^2 - V\,(x_3, x_2, t),
\end{aligned} \tag{4}$$

where the potential V is given as

$$\begin{aligned}
V(x_1, x_3, t) &= \frac{1}{2}m(t)\Bigg\{[\Omega(t) + \xi]\ {x_1}^2\\
&\quad + \frac{\delta(t)}{2}{x_1}^4 - 2\,[\Gamma_1(t) + x_3]\ x_1\Bigg\},\\
V(x_2, x_1, t) &= \frac{1}{2}m(t)\Bigg\{[\Omega(t) + \xi]\ {x_2}^2\\
&\quad + \frac{\delta(t)}{2}{x_2}^4 - 2\,[\Gamma_2(t) + x_1]\ x_2\Bigg\},\\
V(x_3, x_2, t) &= \frac{1}{2}m(t)\Bigg\{[\Omega(t) + \xi]\ {x_3}^2\\
&\quad + \frac{\delta(t)}{2}{x_3}^4 - 2\,[\Gamma_3(t) + x_2]\ x_3\Bigg\}.
\end{aligned} \tag{5}$$

Now, using the well-known Euler-Lagrange equations and considering the restriction $\alpha = 0$ one can rewrite the equation system (2).

For the following steps of this methodology, we focus only on a node x_1, but apply the same steps for the rest of the nodes x_2 and x_3 due to a symmetry in the equations. In the Lagrangian formulation of dynamical systems, the existence of continuous symmetries implies the conservation of certain physical quantities, according to Noether's theorem [18]. To obtain an integral of the motion associated with Eq. (2) are used arguments similar to those employed in Ref. [27]. We consider an infinitesimal transformation of time and the coordinate x_1 of the type:

$$t \mapsto t + \varepsilon\psi(x_1,t), \quad x_1 \mapsto x_1 + \varepsilon\eta(x_1,t),$$

with ε small. This transformation induces the symmetry operator:

$$X = \psi(x_1,t)\,\frac{\partial}{\partial t} + \eta(x_1,t)\,\frac{\partial}{\partial x_1}, \tag{6}$$

which represents an infinitesimal variation of the system.

Applying Noether's theorem requires analyzing how the Lagrangian $L(x_1,\dot{x}_1,x_3,t)$ changes under this transformation. If a given transformation leaves the action integral $S = \int_0^t L(x_1,\dot{x}_1,x_3,t)\,dt$ invariant, then there exists a conserved quantity. This quantity takes the following form:

$$\begin{aligned} Q_1 &= (\psi\dot{x}_1 - \eta)\frac{\partial L(x_1,\dot{x}_1,x_3,t)}{\partial \dot{x}_1} \\ &\quad - \psi L(x_1,\dot{x}_1,x_3,t) + \Gamma_1(t). \end{aligned} \tag{7}$$

Here, the function $\Gamma_1(t)$ is derived from the total derivative added to the non-transformed Lagrangian. Differentiating Eq. (7) with respect to time and setting the result to zero yields a necessary condition for the invariance. This invariance is expressed by the condition:

$$\begin{aligned} &\psi\frac{\partial L(x_1,\dot{x}_1,x_3,t)}{\partial t} + \eta\frac{\partial L(x_1,\dot{x}_1,x_3,t)}{\partial x_1} + \left(\dot{\eta} - \dot{\psi}\dot{x}_1\right) \\ &\times \frac{\partial L(x_1,\dot{x}_1,x_3,t)}{\partial \dot{x}_1} + \dot{\psi}L(x_1,\dot{x}_1,x_3,t) = \dot{\Gamma}_1(t). \end{aligned} \tag{8}$$

In this context, $\dot{\psi}$, $\dot{\eta}$ and $\dot{\Gamma}_1(t)$ are the total variations over time and are given by the following extended derivatives:

$$\begin{aligned} \dot{\psi} &= \frac{\partial \psi}{\partial t} + \frac{\partial \psi}{\partial x_1}\dot{x}_1, \\ \dot{\eta} &= \frac{\partial \eta}{\partial t} + \frac{\partial \eta}{\partial x_1}\dot{x}_1, \\ \dot{\Gamma}_1(t) &= \frac{\partial \Gamma_1(t)}{\partial t} + \frac{\partial \Gamma_1(t)}{\partial x_1}\dot{x}_1. \end{aligned} \tag{9}$$

These expressions allow us to evaluate the complete variation of each term in the invariance equation. Fulfillment of this condition guarantees the existence of a conserved quantity, which in this case is identified as the local energy Q_1 of the corresponding node. In an analogous way, the local energies for Q_2 and Q_3 are obtained, which shows the usefulness of the approach for coupled systems.

$$\begin{aligned} Q_1 &= \frac{1}{2}\left(\rho\dot{x}_1 - \dot{\rho}x_1\right)^2 + \frac{\delta(t)}{4}\rho^2 {x_1}^4 \\ &\quad - \left(\xi x_3 + \Gamma_1(t)\right)\rho^2 x_1 + \frac{K}{2}\left(\frac{x_1}{\rho}\right)^2, \\ Q_2 &= \frac{1}{2}\left(\rho\dot{x}_2 - \dot{\rho}x_2\right)^2 + \frac{\delta(t)}{4}\rho^2 {x_2}^4 \\ &\quad - \left(\xi x_1 + \Gamma_2(t)\right)\rho^2 x_2 + \frac{K}{2}\left(\frac{x_2}{\rho}\right)^2, \\ Q_3 &= \frac{1}{2}\left(\rho\dot{x}_3 - \dot{\rho}x_3\right)^2 + \frac{\delta(t)}{4}\rho^2 {x_3}^4 \\ &\quad - \left(\xi x_2 + \Gamma_3(t)\right)\rho^2 x_3 + \frac{K}{2}\left(\frac{x_3}{\rho}\right)^2. \end{aligned} \tag{10}$$

The integrals of motion Q_1, Q_2 and Q_3 can be interpreted as energies because they are conserved quantities arising from the symmetries of the system, specifically time invariance, according to Noether's theorem. These functions remain constant throughout the evolution of the system and, when expressed in terms of physical variables such as position and velocity, adopt a functional form compatible with kinetic, potential, or total energy. This similarity in their structure and their time conservation are interpreted as energies in classical dynamics.

While this method allows for obtaining a motion integral for (1), the primary focus here is on analyzing the fully coupled system. Furthermore, ρ is a solution to the following Milne-Pinney like equation [31,32]:

$$\ddot{\rho} + \left(\Omega(t) + \xi\right)\rho = \frac{K}{\rho^3}. \tag{11}$$

The function ρ is, in fact, defined in terms of the original function ψ through the relation $\psi = \rho^2$ [31,32]. Additionally, condition (8) implies that the coefficients $\delta(t)$ and $\Gamma_1(t)$, $\Gamma_2(t)$, and $\Gamma_3(t)$ are not free and must satisfy some restrictions given by next expressions:

$$\begin{aligned} \delta(t) &= \frac{C_1}{\rho^6}, \\ \Gamma_1(x_3,t) &= \frac{C_2}{\rho^3} - \xi x_3, \\ \Gamma_2(x_1,t) &= \frac{C_2}{\rho^3} - \xi x_1, \\ \Gamma_3(x_2,t) &= \frac{C_2}{\rho^3} - \xi x_2. \end{aligned} \tag{12}$$

These coefficients mainly depend on the Milne-Pinney solutions, but due to the above mentioned restrictions they also depend on the coupling variable, so Γ_1, Γ_2 and Γ_3 becomes into $\Gamma_1(x_3,t)$, $\Gamma_2(x_1,t)$ and $\Gamma_3(x_2,t)$.

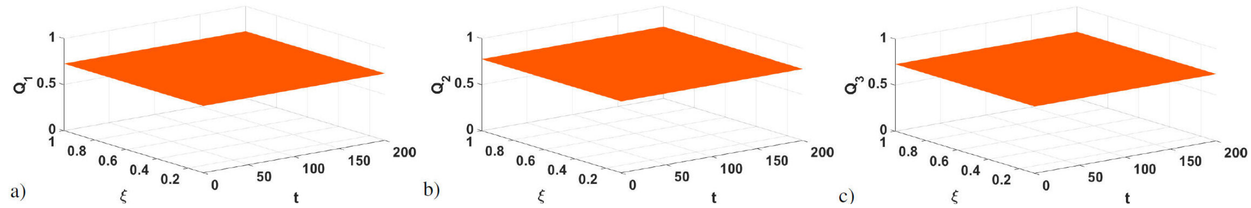

FIGURE 2. A 3D representation of local conservation of the energy Q_j for a) $x_1(t)$, b) $x_2(t)$ and c) $x_3(t)$ in function of coupling strength (ξ) and time (t) for $\Omega = 2$.

3. Numerical results

In order to solve the Eq. (3), the values of the constant coefficients are $C_1 = 1$ related to the nonlinear term, $C_2 = 0.025$ related to the external modulation constant parameter, also $K = 1$ associated with the energy conservation in Eqs. (10). The coupling strength parameter is varied in the range $\xi \in [0, 1]$ and ρ is the solution for Milne-Pinney. Three different cases of natural frequency of oscillation parameter are considered; Case 1: $\Omega = 2$, Case 2: $\Omega(t) = 0.0025\sin(t)$ and Case 3: $\Omega(t) = 0.0025t^2$. The initial conditions are $x_{1,3} = 1/\sqrt{2}$, $x_2 = -1/\sqrt{2}$, and $y_{1,2,3} = 0$.

3.1. Case 1: Constant frequency $\Omega = 2$

Figure 2 presents a three-dimensional visualization of the local energy quantity Q_j corresponding to the state variables $x_1(t)$, $x_2(t)$, and $x_3(t)$, shown in subfigures a), b), and c), respectively. The plots display the dependence of Q_j on the coupling strength ξ and time t, under the condition of a fixed natural frequency $\Omega = 2$. The emergence of flat, constant surfaces across all subfigures indicates the invariance of Q_j with respect to both temporal evolution and variations in ξ. This behavior confirms the local conservation of energy within the system, highlighting the robustness of the dynamical structure and consistency of the theoretical framework employed. The observed invariance further supports the analytical formulation and numerical implementation of the model, demonstrating that local energy conservation is preserved regardless of coupling perturbations within the specified parameter regime.

In Fig. 3, a combined 3D (column I) and 2D (column II) representation illustrates the temporal behavior of the solution to Eq. (3) for the state variables $x_1(t)$, $x_2(t)$, and $x_3(t)$ as functions of the coupling strength ξ, under the condition $\Omega = 2$. The 3D plots (left column) reveal the modulated oscillatory structure of each variable over time and varying coupling, while the 2D plots (right column) allow for a clearer visualization of the frequency and phase synchronization effects induced by changes in ξ.

Figure 4 complements this analysis by presenting the evolution of the local maxima of each state variable with respect to ξ.The amplitude of oscillations indicates that the peak values remain bounded and nearly invariant across the range of coupling strengths considered. These results suggest that the system maintains a periodic and robust oscillatory regime despite variations in the interaction parameter, which is critical for interpreting the underlying dynamics and their potential applications.

Figure 5 illustrates the time series (column I) and phase portraits (column II) of $x_1(t)$ for varying values of the coupling parameter ξ. As ξ increases from 0.1 to 1.0, a noticeable trend can be observed in both the amplitude and the phase space trajectories. At lower values of ξ [panels a) and b)], the system exhibits high-amplitude oscillations with relatively broad phase portraits, indicating strong periodic behavior and limited damping. As ξ approaches intermediate

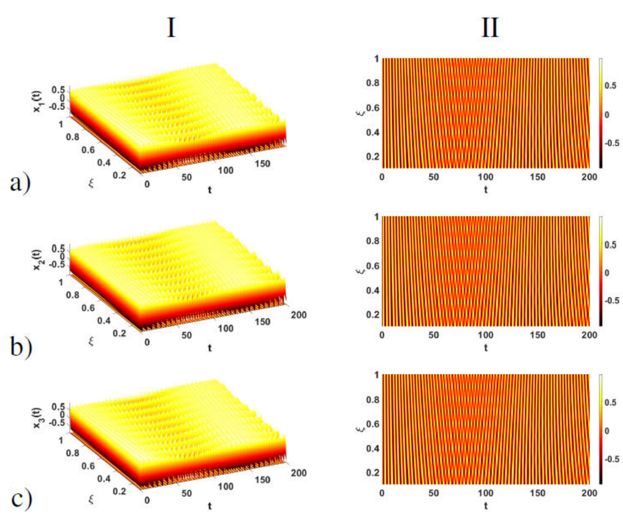

FIGURE 3. A (I) 3D and (II) 2D representation of temporal behavior of (3) for a) $x_1(t)$, b) $x_2(t)$ and c) $x_3(t)$ in function of coupling strength (ξ) for $\Omega = 2$.

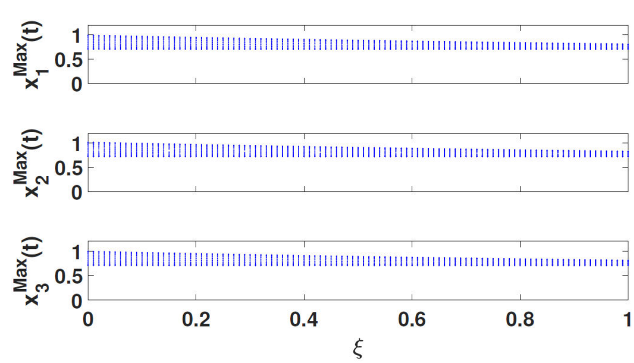

FIGURE 4. Local maximum for $x_1(t)$, $x_2(t)$ and $x_3(t)$ in function of coupling strength (ξ) $\Omega = 2$.

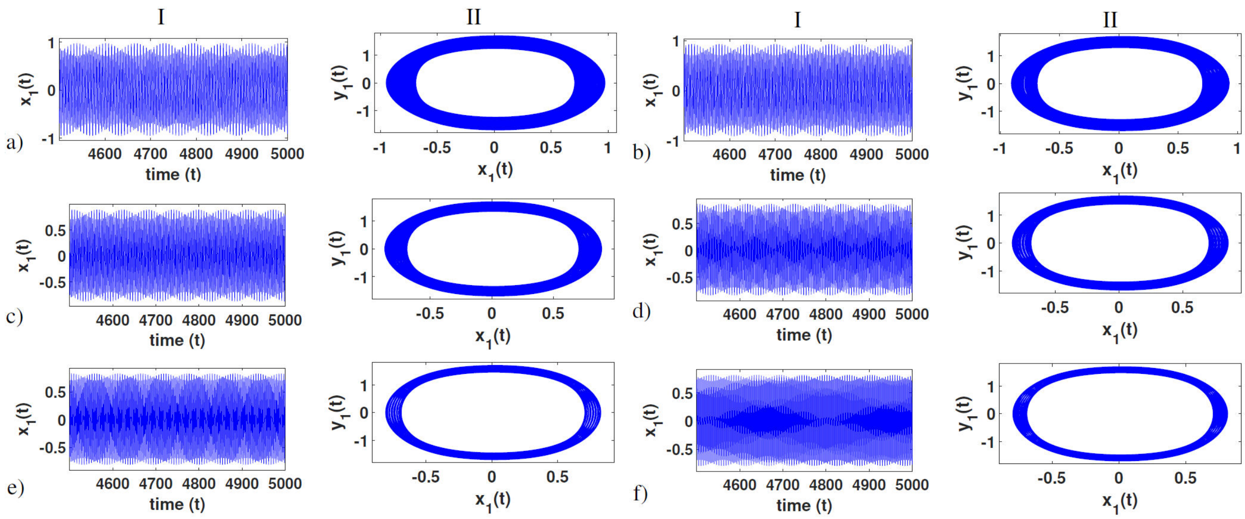

FIGURE 5. (I) Time series and (II) phase portrait of $x_1(t)$ for a) $\xi = 0.1$, b) $\xi = 0.3$, c) $\xi = 0.5$, d) $\xi = 0.5$, e) $\xi = 0.7$, f) $\xi = 0.9$ and $\xi = 1.0$ for $\Omega = 2$.

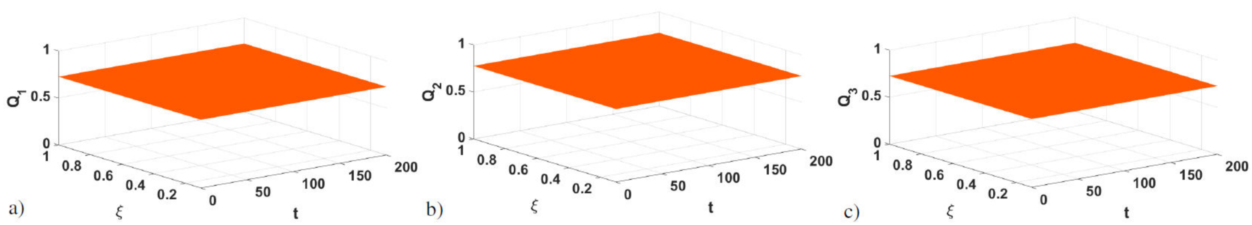

FIGURE 6. A 3D representation of local conservation of the energy Q_j for a) $x_1(t)$, b) $x_2(t)$ and c) $x_3(t)$ in function of coupling strength (ξ) and time (t) for $\Omega(\mathrm{t}) = 0.0025\sin(t)$.

values [panels c) and d)], the amplitude becomes more stabilized, and the phase portraits maintain a more consistent elliptical shape, suggesting a balance between coupling and damping effects. At higher ξ values [panels e) and f)], the amplitude of oscillations decreases slightly, and the phase portraits become tighter, indicating enhanced damping and

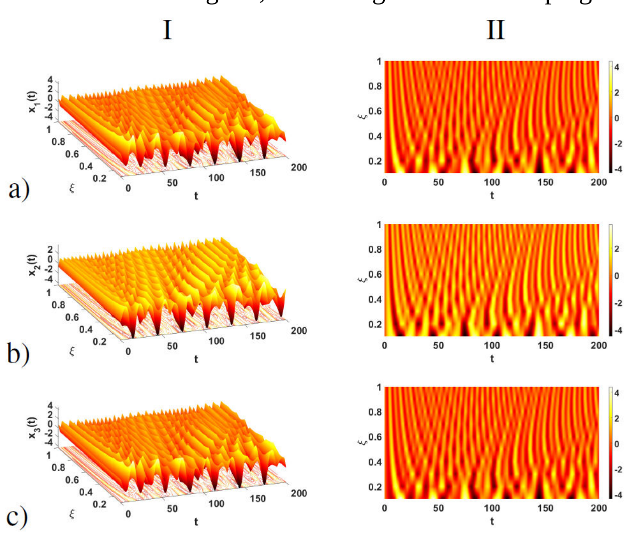

FIGURE 7. A (I) 3D and (II) 2D representation of temporal behavior of (3) for a) $x_1(t)$, b) $x_2(t)$ and c) $x_3(t)$ in function of coupling strength (ξ) for $\Omega(\mathrm{t}) = 0.0025\sin(t)$.

reduced oscillatory energy. These observations suggest that increasing ξ leads to a gradual transition from strong periodicity towards more damped oscillatory dynamics, reflecting the critical role of coupling strength in the system's behavior.

3.2. Case 2: Sinusoidal frequency $\Omega = 0.0025\sin(t)$

Figure 6 displays the three-dimensional behavior of the local energy functions Q_j associated with the state variables $x_1(t)$, $x_2(t)$, and $x_3(t)$, as depicted in subfigures a), b), and c), respectively. The analysis is carried out under the condition of a time-dependent frequency $\Omega(t) = 0.0025\sin(t)$. Despite

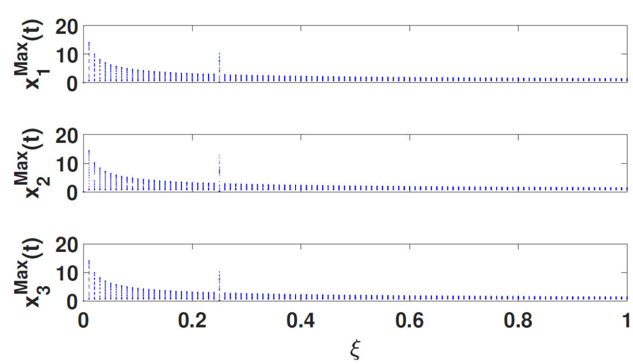

FIGURE 8. Local maximum for $x_1(t)$, $x_2(t)$ and $x_3(t)$ in function of coupling strength (ξ) $\Omega(\mathrm{t}) = 0.0025\sin(t)$.

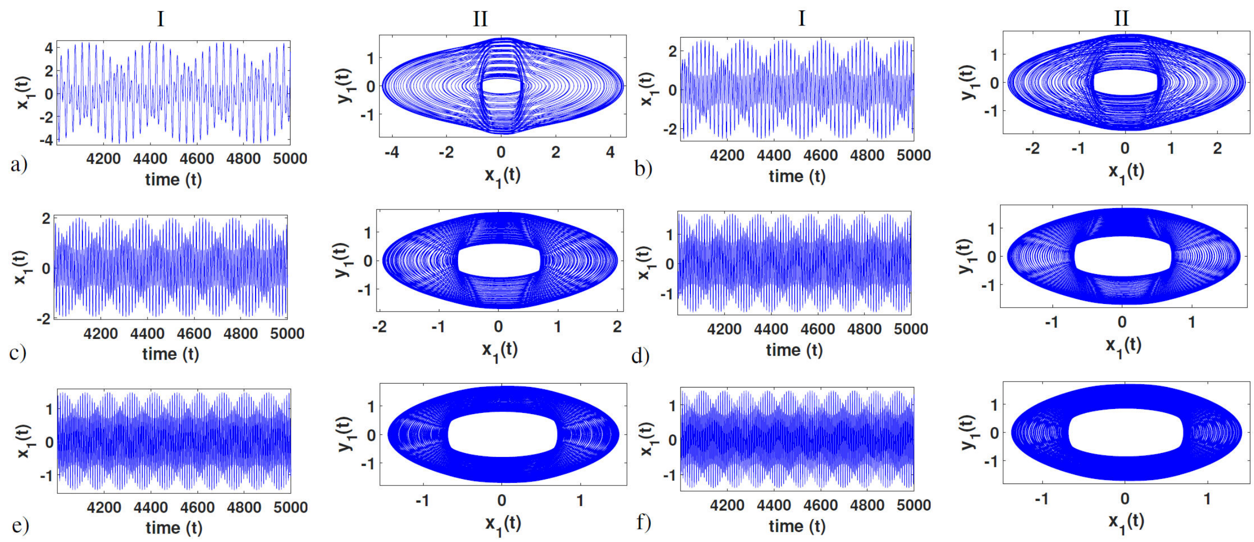

FIGURE 9. (I) Time series and (II) phase portrait of $x_1(t)$ for a) $\xi = 0.1$, b) $\xi = 0.3$, c) $\xi = 0.5$, d) $\xi = 0.5$, e) $\xi = 0.7$, f) $\xi = 0.9$ and $\xi = 1.0$ for $\Omega(\mathrm{t}) = 0.0025\sin(t)$.

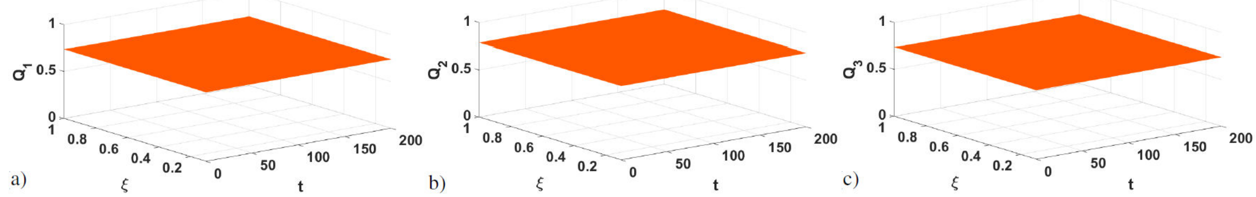

FIGURE 10. A 3D representation of local conservation of the energy Q_j for a) $x_1(t)$, b) $x_2(t)$ and c) $x_3(t)$ in function of coupling strength (ξ) and time (t) for $\Omega(\mathrm{t}) = 0.0025t^2$.

the introduction of temporal variability in the system's frequency, the resulting surfaces remain perfectly flat across both time t and coupling strength ξ, indicating strict conservation of the local energy quantities Q_j. This result strongly supports the robustness of the local conservation property under non-autonomous conditions and reinforces the internal consistency of the dynamical framework. The invariance of Q_j in this non-stationary regime suggests that the formulation preserves key structural symmetries responsible for the conservation laws.

Figure 7 displays both three-dimensional (column I) and two-dimensional (column II) representations of the time evolution of $x_1(t)$, $x_2(t)$, and $x_3(t)$ as functions of the coupling strength ξ. Compared to the autonomous case, the oscillatory patterns become more irregular and exhibit amplitude modulations due to the sinusoidal variation in frequency, suggesting sensitivity to the non-autonomous perturbation.

Figure 8 shows the local maxima of the state variables as a function of ξ, revealing sharp discontinuities and irregular structures. These abrupt changes in peak amplitude reflect transitions under a transition at the coupling threshold, where the time evolution and phase space stabilize at a frequency phenomenon induced by the periodicity in $\Omega(t)$.

Figure 9 presents the time series (column I) and phase portraits (column II) of $x_1(t)$ for different values of ξ. The phase space trajectories reveal a transition from nearly har-

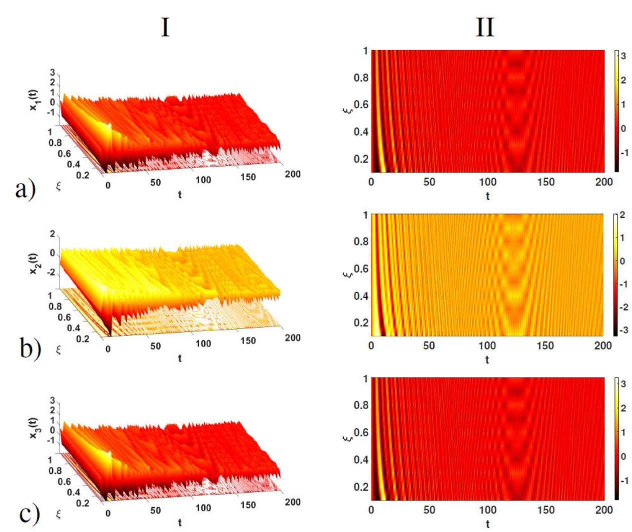

FIGURE 11. A (I) 3D and (II) 2D representation of temporal behavior of (3) for a) $x_1(t)$, b) $x_2(t)$ and c) $x_3(t)$ in function of coupling strength (ξ) for $\Omega(\mathrm{t}) = 0.0025t^2$.

monic motion to more complex, flattened, or elliptical loops as ξ increases. This deformation of orbits suggests a shift in the system's dominant frequencies or the onset of nonlinear effects, despite the conservation of local energy. Together, these results emphasize the rich and sensitive dynamical response introduced by non-autonomous forcing, highlighting

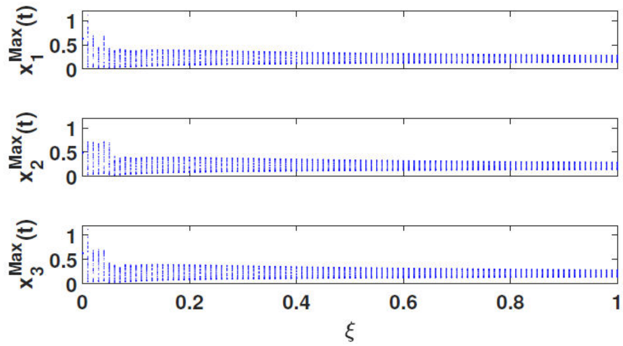

FIGURE 12. Local maximum for $x_1(t)$, $x_2(t)$ and $x_3(t)$ in function of coupling strength (ξ) $\Omega(\mathrm{t}) = 0.0025t^2$.

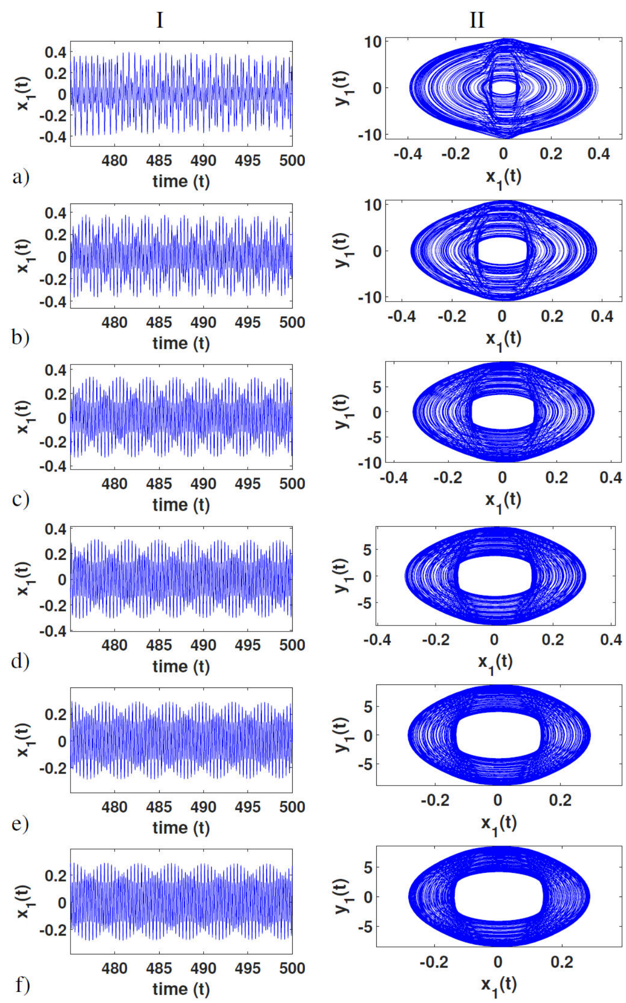

FIGURE 13. (I) Time series and (II) phase portrait of $x_1(t)$ for a) $\xi = 0.1$, b) $\xi = 0.3$, c) $\xi = 0.5$, d) $\xi = 0.5$, e) $\xi = 0.7$, and f) $\xi = 0.9$ $\xi = 1.0$ for $\Omega(\mathrm{t}) = 0.0025t^2$.

the necessity of time-varying analysis in systems with modulated parameters.

3.3. Case 3: Quadratic frequency $\Omega = 0.0025t^2$

In Fig. 10, the local energy Q_j is shown to remain constant across time and coupling strength ξ, confirming that local conservation persists even in the presence of accelerated forcing. Despite this conservation, the system displays increasingly complex behavior.

Figure 11 illustrates the temporal evolution of $x_1(t)$, $x_2(t)$, and $x_3(t)$, showing a progressive densification of the oscillatory patterns with time. Initially, the trajectories present lower frequency oscillations, but as the system evolves, an intensification of the temporal variability is observed, manifested by steeper slopes in the curves. This behavior suggests the presence of high-frequency components in the system dynamics, originating from the quadratic influence of $\Omega(t)$, which introduces a temporal variation in the structure of the interaction compared with the other cases. Furthermore, the coupling strength ξ intervenes by modulating the amplitude and stability of these oscillations, suggesting a transition towards a more complex behavioral regime.

The analysis of local maxima presented in Fig. 12 shows a sharp increase in the number and irregularity of peaks as ξ varies, indicating enhanced sensitivity to coupling under quadratic modulation.

Figure 13 shows the time series and phase portraits of $x_1(t)$ for different values of ξ. As ξ increases, the phase trajectories gradually deform from smooth closed orbits to more compressed and irregular loops. The corresponding time series reflect a progression toward richer and more intricate waveforms, highlighting the influence of both strong coupling and nonlinearly increasing frequency on the global structure of the solution. These observations collectively demonstrate that quadratic modulation of the driving frequency significantly enhances the dynamical complexity of the coupled Duffing oscillators.

In summary, numerical simulations demonstrate that although local energy conservation Q_j is strictly preserved in all tested cases, the system's qualitative dynamics are strongly influenced by the external driving frequency's profile $\Omega(t)$ and the coupling parameter ξ. When the frequency shifts from a constant value to sinusoidal and quadratic variations, the system progresses from simple harmonic motion to more intricate, high-frequency oscillations, accompanied by significant shifts in amplitude behavior and phase-space trajectories. These results highlight the complex relationship between coupling effects and external forcing in determining the spatiotemporal evolution of coupled Duffing oscillators, providing key insights into nonlinear energy transfer mechanisms in conservative systems.

4. Conclusion

This work shows that the analysis of a system of three nonautonomous, forced, undamped, and unidirectionally linked Duffing oscillators provides valuable insights into local energy conservation in nonlinear dynamical systems. By applying the Milne-Pinney equations, solutions to the system were derived, enabling a thorough examination of its time-dependent behavior and revealing the specific scenarios where energy is locally conserved at certain points in the tri-coupled ring structure. These findings are particularly significant as they highlight how one-way coupling, in the presence of non-autonomous terms, can lead to diverse dynamical behaviors, affecting the local energy distributions at each node depending on the diffusive coupling. Unlike linear systems or conventional models, these oscillators exhibit intricate interactions, underscoring the crucial role of local energy conservation in understanding complex nonlinear dynamics. This work extends the theoretical framework for coupled dynamical systems by demonstrating that energy conservation is not simply a global phenomenon, but can manifest itself in localized regions under specific structural and association conditions, which could inform future research on energy transfer and control strategies for nonlinear systems.

Acknowledgments

Two of us, Alvarado-López and Carmona-Moreno, thank the Secretary of Science, Humanities, Technology and Innovation (SECIHTI) for the financial support granted through the scholarships 2054214 and 2054411, respectively.

1. G. Duffing, Erzwungene Schwingungen bei veränderlicher Eigenfrequenz und ihre technische Bedeutung, 41-42 (Vieweg, 1918).
2. A. H. S. Salas, J. E. C. Hernandez, and L. J. M. Hernandez, The Duffing Oscillator Equation and Its Applications in Physics, *Mathematical Problems in Engineering* **2021** (2021) 1, https://doi.org/10.1155/2021/9994967
3. N. H. Aljahdaly and S. A. El-Tantawy, On the Multistage Differential Transformation Method for Analyzing Damping Duffing Oscillator and Its Applications to Plasma Physics, *Mathematics* **9** (2021) 432, https://doi.org/10.3390/math9040432.
4. A. Gusso, S. Ujevic, and R. L. Viana, Strong chaotification and robust chaos in the Duffing oscillator induced by two-frequency excitation, *Nonlinear Dynamics* **103** (2021) 1955, https://doi.org/10.1007/s11071-020-06183-4.
5. Y. Lei and F. Guan, Disorder induced order in an array of chaotic Duffing oscillators, *International Journal of Modern Physics C* **23** (2012) 1250071, https://doi.org/10.1142/S0129183112500714.
6. Y. Liu *et al*., Complex Periodic Motions and Bifurcations of a Forced Duffing Oscillator with Its Field-Programmable Gate Arrays Implementation, *Applied Sciences* **14** (2024) 11243, https://doi.org/10.3390/app142311243
7. P. Hui and Z. Wei, Laser Ultrasonic Weak Defect Signal Detections Based on Duffing Oscillator, *Russian Journal of Nondestructive Testing* **61** (2025) 23, https://doi.org/10.1134/S1061830924602253
8. V. Gubbi *et al*., Bio-inspired acoustic MEMS sensor with tunable resonance frequency, *Sensors and Actuators A: Physical* **387** (2025) 116369, https://doi.org/10.1016/j.sna.2025.116369.
9. H. Yang, B. Liu, and G. Li, High-order double-coupled Duffing oscillator system with additional damping term and its application in ship-radiated noise signal detection, *The European Physical Journal Plus* **139** (2024) 662, https://doi.org/10.1140/epjp/s13360-024-05451-1
10. N. Q. Hu and X. S. Wen, The application of Duffing oscillator in characteristic signal detection of early fault, *J. Sound and Vibration* **268** (2003) 917, https://doi.org/10.1016/S0022-460X(03)00002-6.
11. R. F. Fonkou and M. A. Savi, Heart Rhythm Analysis Using Nonlinear Oscillators with Duffing-Type Connections, *Fractal and Fractional* **7** (2023) 592, https://doi.org/10.3390/fractalfract7080592
12. T. Murakami *et al*., Study on detection of epileptic discharges based on a Duffing oscillator model, *Tech. rep., IMECE* (2014), https://doi.org/10.1115/IMECE2014-38107
13. I. Kovacic and M. J. Brennan, The Duffing equation: nonlinear oscillators and their behaviour (John Wiley and Sons, 2011).
14. J. Barba-Franco *et al*., Dynamics of a ring of three unidirectionally coupled Duffing oscillators with time-dependent damping, *Europhysics Letters* **134** (2021) 30005, https://doi.org/10.1209/0295-5075/134/30005.
15. J. Barba-Franco *et al*., Dynamics of a ring of three unidirectionally coupled Duffing oscillators with time-dependent damping, Europhysics Letters **134** (2021) 30005, https://doi.org/10.1209/0295-5075/134/30005
16. U. Uriostegui-Legorreta and E. S. Tututi, Synchronization in the van der Pol-Duffing system via elastic and dissipative couplings, *Rev. Mex. Fis.* **68** (2021) 1, https://doi.org/10.31349/RevMexFis.68.011402
17. S. Balaraman *et al.*, From coexisting attractors to multispiral chaos in a ring of three coupled excitation-free Duffing oscillators, *Chaos, Solitons and Fractals* **172** (2023) 113619, https://doi.org/10.1016/j.chaos.2023.113619
18. E. Noether, Invariante variationsprobleme, In Gesammelte Abhandlungen-Collected Papers, pp. 231-239 (Springer, 1983).
19. S. Nemat-Nasser, Mechanics Today: Pergamon Mechanics Today Series (Elsevier, 2014).
20. J. La Salle and S. Lefschetz, Stability by Liapunov's direct method (Academic Press, 1961).
21. N. G. Chetaev *et al*., The stability of motion (Pergamon Press, 1961).
22. B. C. Xanthopoulos, Integrals of motion and analytic functions, *Journal of Physics A: Mathematical and General* **17** (1984) 87, https://doi.org/10.1088/0305-4470/17/1/011.
23. Y. Kosmann-Schwarzbach, The Noether theorems (Springer, 2011).

24. B. Haq and I. Naeem, First integrals and analytical solutions of some dynamical systems, *Nonlinear Dynamics* **95** (2019) 1747, https://doi.org/10.1007/s11071-018-4657-4.

25. M. R. C. Da Silva, A transformation approach for finding first integrals of motion of dynamical systems, *International Journal of Non-Linear Mechanics* **9** (1974) 241, https://doi.org/10.1016/0020-7462(74)90039-0.

26. J. Baumgarte, Stabilization of constraints and integrals of motion in dynamical systems, *Computer methods in applied mechanics and engineering* **1** (1972) 1, https://doi.org/10.1016/0045-7825(72)90018-7.

27. E. Urenda-Cázares *et al*., Integral of motion and nonlinear dynamics of three Duffing oscillators with weak or strong bidirectional coupling, *Nonlinear Dynamics* **111** (2023) 18953, https://doi.org/10.1007/s11071-023-08893-x

28. J. de Jesús Barba-Franco *et al*., An integral of motion for a Master-Slave system of damped Duffing oscillators with variable coefficients: Nonlinear dynamics and computer simulations, *International Journal of Modern Physics C* **35** (2024) 2450150, https://doi.org/10.1142/S012918312450150X.

29. L. M. Pecora and T. L. Carroll, Synchronization of chaotic systems, *Chaos* **25** (2015) 097611, https://doi.org/10.1063/1.4917383.

30. A. F. Vakakis *et al.*, Nonlinear targeted energy transfer in mechanical and structural systems (Springer Dordrecht, 2008), https://doi.org/10.1007/978-1-4020-9130-8.

31. W. E. Milne, The Numerical Determination of Characteristic Numbers, *Physical Review* **35** (1930) 863, https://doi.org/10.1103/PhysRev.35.863

32. E. Pinney, The nonlinear differential equation y" + p(x)y + cy^{-3} = 0, *Proceedings of the American Mathematical Society* **1** (1950) 681, https://doi.org/10.1090/s0002-9939-1950-0037979-4